Nuclear Inst. and Methods in Physics Research, A 922 (2019) 19–27

Contents lists available at ScienceDirect

Nuclear Inst. and Methods in Physics Research, A

journal homepage: www.elsevier.com/locate/nima

Associated particle imaging instrumentation for future planetary surface missions

M.L. Litvak [a,*], Y.N. Barmakov [b], S.G. Belichenko [b], R.R. Bestaev [b], E.P. Bogolubov [b], A.V. Gavrychenkov [b], A.S. Kozyrev [a], I.G. Mitrofanov [a], A.V. Nosov [a], A.B. Sanin [a], V.N. Shvetsov [c], D.I. Yurkov [b], V.I. Zverev [b]

[a] Space Research Institute, RAS, Moscow, 117997, Russia
[b] Federal State Unitary Enterprise «All-Russia Research Institute of Automatics n.a. N.L. Dukhov» (VNIIA), Moscow, Russia
[c] Joint Institute for Nuclear Research, Dubna, Russia

ARTICLE INFO

Keywords:
Tagged neutrons method
Associated particle imaging
Active gamma spectroscopy
Neutron generator
Elemental abundances
Solar system
Surface operations

ABSTRACT

We have conducted ground tests to study the applicability of the Tagged Neutrons Method/Associated Particle Imaging methodology (TNM/API) for the making precise gamma ray spectroscopic measurements onboard lander missions to the Solar system planets. Our analysis was focused on the requirement to distinguish between the spacecraft background and the subsurface signal so as to correctly evaluate the elemental composition of planetary soils. The measurements were performed in a configuration where the gamma spectrometer was surrounded by significant amounts of material that imitated a spacecraft structure. It was found that the TNM/API can substantially suppress the spacecraft background and identify the true intensities of the gamma lines attributed to major soil elements such as O, Na, Mg, Al, Si and Fe and evaluate their concentrations with an accuracy of 2–10%.

1. Introduction

Gamma-ray and neutron spectroscopy instrumentation are often proposed for space experiments to derive the bulk elemental composition of a planetary subsurface. They have a long history of successful implementation onboard different missions dedicated to the study of Solar system [see for example [1–12]]. These have usually been orbital missions selected to provide global mapping of planetary surfaces and to evaluate the elemental composition and abundance of subsurface water. At the present time there is great interest in the science community to measure the local ambient environment at the surface, to carry out complex contact (including sampling analysis) measurements, and to compare orbital and surface data. These requirements lead to the consideration, planning, and development of major flagship missions culminating in surface landers on planets, moons, and other small bodies in the Solar system. Some of these projects are already in progress like NASA Curiosity rover [13]. Some are at the final development stage like the ExoMars [14] and NASA Mars 2020 rovers or lunar landing missions prepared by other national space agencies.

As a rule, landing missions are often equipped with neutron and gamma spectrometers for measuring subsurface composition and to support/navigate drilling and sampling activities. The neutron spectrometers measure variations in subsurface neutron albedo that can be converted into water abundance. Gamma spectrometers detect characteristic gamma-ray lines originating from major soil constituents (O, Na, Mg, Al, Si, Ca, K, and Fe). The natural neutron emission of the subsurface is produced by Galactic Cosmic Ray charged particles which interact with soil nuclei giving birth to secondary neutrons. The characteristic gamma ray lines in their turn are emitted from the de-excitation of soil nuclei through nuclear reactions with these neutrons. These could be from inelastic scattering via reactions with fast neutrons or neutron capture reactions with low energy thermal/epithermal neutrons or even neutron activation reactions. This approach is unofficially referred to as a form of “passive observation”. It uses natural radiation background as the irradiation source. Induced subsurface gamma emission can also be produced by artificial irradiation sources, for example, by neutron generators. These sources produce very intense pulses or continuous emissions of high energy neutrons using Deuterium–Tritium (D–T) or Deuterium–Deuterium (D–D) reactions. This “active approach” significantly improves counting statistics and reduces the time required for gamma spectroscopy measurements to obtain a given accuracy. The combination of gamma/neutron spectrometers with a neutron generator is commonly used in geology, security, transportation, medicine, and other Earth applications. It has also been proposed for space studies [15–28] with the first active neutron spectrometer already operating onboard the NASA Curiosity rover [20,29–33]. In general, the idea of

* Corresponding author.
E-mail address: litvak@mx.iki.rssi.ru (M.L. Litvak).

https://doi.org/10.1016/j.nima.2018.11.050
Received 8 August 2018; Received in revised form 9 November 2018; Accepted 10 November 2018
Available online 14 November 2018
0168-9002/

active measurements in space was proposed many years ago but only recently have we achieved the necessary technology level to develop compact and reliable instrumentation for such purposes [see for example [24,25]].

A gamma-ray spectroscope allows us to "look inside" an object and derive information about its inner properties. As was mentioned above, in the case of space experiment, it can be used to determine the bulk elemental composition of the object which is not possible using other observational approaches. On the other hand, one must be ready "to pay" for this advantage by simultaneously measuring the parasite background gamma emissions originating from the spacecraft body. For passive observations it is not possible to distinguish between spacecraft and subsurface signals without sophisticated ground calibrations. In any case, even knowing the ratio between these components ultimately cannot exclude significant background deposits from the signal-to-noise ratio.

For active observations it also presents a difficulty but there are techniques that allow one to restrict gamma detection to a limited solid angle. This technique is known as the associated particle imaging (API) or tagged neutron method (TNM) which has been implemented widely by industry, primarily for security applications to detect hidden dangerous materials [2,28,34–38]. This approach selects gammas produced in the object under study and rejects gamma detections from the surroundings. Using this method, one can significantly maximize the signal-to-noise ratio and reveal some gamma lines usually not visible above background levels.

Studying this problem, it is necessary to answer to the following questions:

(1) How the signal-to-noise ratio and, as a result, the achievable uncertainty in the evaluation of subsurface elemental concentrations is getting worse in the presence of a massive spacecraft body.
(2) How the parasitic background produced in the surrounding spacecraft materials may complicate the search, selection, and correct interpretation of gamma peaks intensities for the primary elemental soil constituents.
(3) How the TNM/API method could significantly improve the situations outlined in (1) and (2) and make its implementation in space experiments worthwhile.

In this work we will report results of ground tests performed on a planetary soil simulant with a prototype of the spectrometer using TNM/API measurements. In our tests we modeled both the soil's elemental composition and the lander's surrounding materials to evaluate the benefits of TNM/API for the planetary studies.

2. Instrumentation

The instrumentation for the (TNM/API) consists of a combination of gamma-ray spectrometer and neutron generator supplied with a position-sensitive alpha particle detector. The neutron generators used in most applications are based on the nuclear fusion reaction T(d,n) ^{4}He which produces fast neutron and alpha particles with energies of 14 MeV and 3.5 MeV respectively. Taking into account that reaction products (neutron and alpha particle) are flying apart in opposite directions, the registration of alpha particle with position sensitive detector determines the time and direction of the fast neutron emitted from the tritium target. This neutron (it travels with constant velocity of about 5 cm/ns) in its turn may interact with the nuclei of the sample material via inelastic scattering reactions and produce a characteristic gamma photon. The accurate measurement of time interval between detections of the alpha particle and the gamma photon provides information about a location where the interaction between the neutron and the target's nucleus occurred. The selection of photons produced only by tagged neutrons and arriving from the estimated distances drastically reduces the parasitic background rate from the surrounding material by orders of magnitude. To implement TNM, a pixilated alpha detector should be used and a correlation analysis performed with nanosecond timing resolution. For the last decade TNM has been widely implemented for multiple purposes that range from the detection of explosives and drug materials up to the search for diamonds in kimberlite [see for example [35–39]]. For our studies we used a neutron generator ING-27 developed by the Dukhov Research Institute of Automatics (VNIIA) and is equipped with a 9-pixel silicon alpha particular detector. The distance of the alpha detector from the tritium target varies for different models of the neutron generator and can lie in the range from 30 mm to 100 mm. In ING-27 used in this work, the distance was 63 mm. This is a commonly used industrial type of neutron generator which has relatively compact dimensions (130 × 280 × 230 mm), low mass (less than 8 kg) and can provide continuous neutron emission with an intensity 10^6–10^8 neutrons/s.

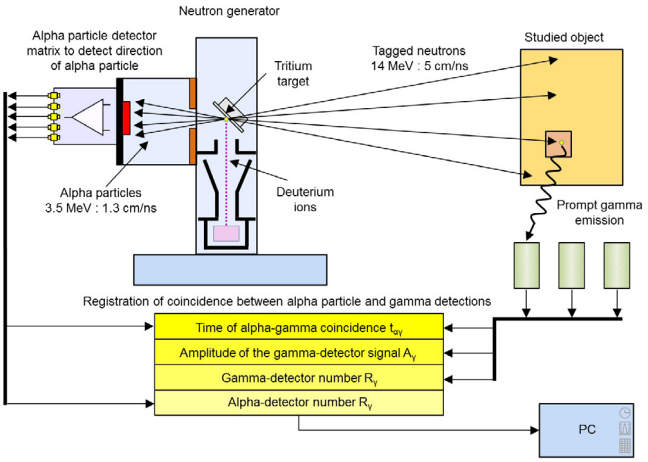

Fig. 1. Schematic illustration of the TNM/API approach.

The measurement system also includes an instrument electronic unit and two gamma-ray spectrometers based on $LaBr_3$(Ce) and LYSO ($Lu_{1.8}Y_{.2}SiO_5$:Ce) scintillation crystals with dimensions Ø × L = 76 × 76 mm manufactured by Saint-Gobain company. The first one provides better spectral resolution (about 3% at 662 keV) and the other one has better sensitivity at high energies (but worse spectral resolution). In the process of taking data, the electronics records the triggered pixel in the alpha particle detector, the times of the alpha particle and gamma detections (t_α, t_γ,), and the energy of the detected gamma photon (E_γ). These values are processed to create integrated gamma-ray spectra from the irradiated planetary soil simulant. Schematically the measurements with the use of TNM/API methods are illustrated in Fig. 1.

3. Test configuration

All tests were conducted at the Joint Institute for Nuclear Research (JINR) in Dubna, Russia, with the help of a facility specially designed for ground tests of space instrumentation using radioisotope neutron sources, neutron generators, and neutron/gamma-ray spectrometers [18,23,33,40]. The facility has a large testbed of planetary simulant material with a surface area of 3.21 m × 3.83 m and a depth >60 cm. The planetary simulant material is assembled as a multilayered structure of 10 mm layers of silicon rich glass and 0.7–1 mm layers of Fe and Al enriched material and polyvinylchloride (Cl rich material) designed to achieve an elemental composition close to the average composition of dry martian soil [Table 1, column 1, see also [18,23,40] for details]. It imitates the average abundance of major soil constituting elements Si, O, Al, Mg, Fe, K, Cl, and Na. The structure is changeable and can be adapted to the different compositions of Mars, Moon, Mercury, Venus, and asteroids/comets.

Table 1
The expected uncertainties in the evaluation of major soil constituting elements.

Element	TNM/API measurements		NRA measurements		Comments
	"no Lander" configuration	"Lander" configuration	"no Lander" configuration	"Lander" configuration	
Al/Fe (5.0%/12.5%)	4.7%	4.7%	3.1%	4.6%	Al gamma line at 844 keV; Fe gamma line at 847 keV
Al (5.0%)	10.4%	10.5%	6.5%	9.7%	Al gamma line at 1015 keV
Na (8.4%)	8.0%	8.5%	–	–	Na gamma line at 1636 keV
Si (26.7%)	1.9%	1.9%	2.5%	3.8%	Si gamma line at 1779 keV
Al (5.0%)	9.0%	10.0%	5.0%	7.8%	Al gamma line at 2211 keV. For the NRA it may overlaps with H neutron capture gamma line at 2223 keV
Mg/O (2.4%)	8.0%	9.0%	7.2%	11.1%	Mg gamma line at 2754 keV O gamma line at 2742 keV

The concentrations of different elements in soil simulant material are presented in first column in brackets.
The presented uncertainties in 2nd–5th columns have been calculated in accordance with Eq. (1).
The uncertainty estimations for NRA measurements in "Lander" configuration (5th column) are calculated with elimination of spacecraft component from gamma peak intensity.
Na gamma peak at 1636 keV is not well defined in NRA spectra.
Some gamma peaks overlap each other, and multi-component analysis is required to distinguish concentration of the particular element.

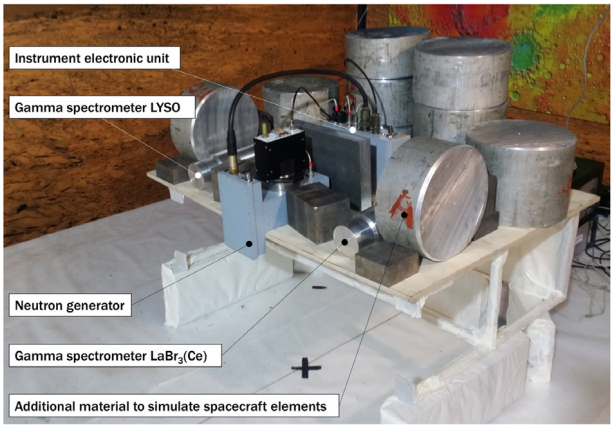

Fig. 2. Photo of the "Lander" ground test configuration.

Originally the planetary simulant model consisted only of dry materials with a hydrogen concentration of less than 0.4% water equivalent. It can also imitate water/water ice depth distribution by adding a 10 mm polyethylene layers inside the simulant model structure [18,23]. For our experiment we used martian soil models where the water/water ice layer (~5 cm) was located beneath the surface at depths of 5–10 cm.

The main goal of the ground tests performed was to simulate surface operations during a landing mission on another planet and to understand how TNM/API could improve the identification of the bulk elementary composition of the planetary soil. We have added additional complexity to the test configuration as compared to our previous measurements, see [18,23,40]. Two different test cases were conducted.

For the first one (the so called "no lander" configuration), the whole measurement system including $LaBr_3$(Ce), LYSO, Neutron generator (NG), and the instrument electronics unit was set up above the planetary simulant material on a special mechanical frame to simulate a probable configuration onboard a lander. This configuration takes into account the possible distance between the NG and GRS inside the lander and the elevation above the ground. Both gamma spectrometers were placed symmetrically to different sides of the NG at distances of about 30 cm. The elevation above the ground was also selected to be 50 cm.

The second configuration (the so called "lander" configuration) was produced from the previous one by adding surrounding material to imitate the spacecraft shell/chassis around the science instrumentation. In total, we used several hundred kilos of aluminum alloys (99.3% of Al, ~0.3% of Si, and ~0.3% of Fe) placed around the measurement system to represent spacecraft material. A photo of the "lander" configuration is presented in Fig. 2.

The measurement system allows both operations using the TNM/API method as well as measurements in a mode with the correlation between detections of alpha particles/neutrons and gamma photons disabled. It allows us the possibility of comparing the gamma spectra from the planetary soil material obtained with and without (standard neutron radiation analysis) implementing the TNM/API method and compares the identification of the primary gamma lines (produced by the most abundant soil elemental constituents) by both types of measurements.

For each test configuration we conducted TNM/API measurements for one hour and a standard neutron radiation analysis for 5 min. The duration of the TNM/API measurement was selected to be as long as possible to get maximal counting statistics. It was based on our operational experience in using the neutron generator on the MSL Curiosity. Future Venus landing missions proposals also reference it as the maximal possible time for NG surface operations on Venus due to the limited lifetime in the harsh temperature and pressure environment. For stationary landing platforms (e.g., for missions to Mars and Moon), this measurement time could be significantly larger if the mission is able to operate for several hundred days. The duration of the standard neutron radiation measurement was selected to get approximately the same total counting statistics as for the TNM/API measurements. That requires at least 10 times less accumulation time.

In concluding this section, we note that the overall test program included 4 primary measurements: 2 per each test configuration plus a set of service and commissioning measurements to tune and calibrate the measurements system. The commissioning measurements included calibration of the gamma ray spectrometers' spectral channels vs energy and the evaluation of the energy dependent resolution of the scintillation crystals. The measurements were used to the compare signal-to-noise ratio and the capability to identify/separate different gamma lines for TNM/API method and for the standard neutron radiation approach (NRA) for "no lander" and "lander" configurations.

4. Results and discussion

The implementation of TNM/API requires complicated timing analyses based on the registration of coincidences between alpha particle and gamma detections. In Fig. 3 we show the time profile of the gamma counting rate synchronized relative to the detection of the alpha particle in the selected segments of the alpha particle detector. The synchronization means that the zero on the time axis presented in Fig. 3 corresponds to the time of the alpha particle detection. The segment selection for the alpha particle detector is required to identify only alpha particle (and hence fast neutrons) trajectories within a certain solid

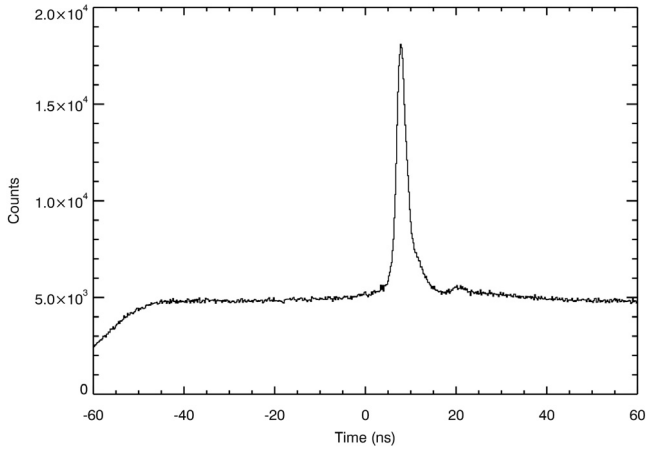

Fig. 3. Time profile of the counting rate illustrating the coincidence algorithm between the detection of the alpha particle and the gamma photon produced in the planetary soil simulant.

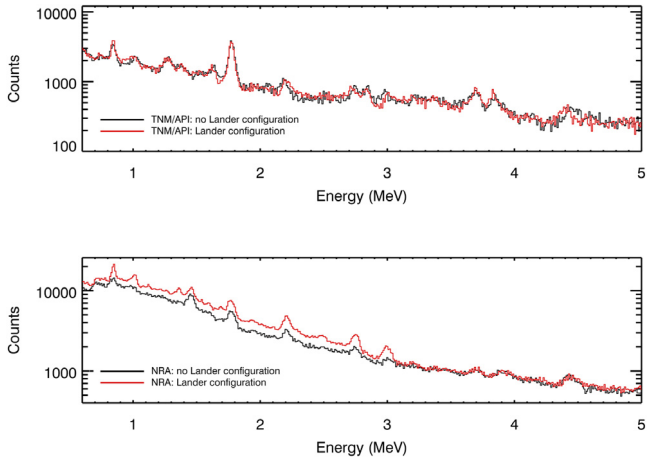

Fig. 4. Integrated gamma spectra measured by the TNM/API (top graph) and the NRA methods for the "lander" (red color) and the "no lander" (black color) configurations . (For interpretation of the references to color in this figure legend, the reader is referred to the web version of this article.)

angle cone. For the tests we have selected a solid angle cone covering the surface area spot located just under the NG (see the "cross" mark in Fig. 2). The diameter of the ground spot is about 25 cm.

In the TNM/API operation mode, the measurements system continuously records the gamma counting rate in the memory buffer with nanosecond accuracy. It provides the possibility to estimate the gamma counting rate before (the memory buffer records about 60 ns) and after the moment of alpha particle detection. That is why one can see negative times on Fig. 3. The main sharp peak on the profile corresponds to the time interval between when the gamma photons are produced in the subsurface by fast neutrons (inelastic scattering reactions) and their arrival at the gamma spectrometer volume. The peak is shifted by ~8 ns from zero due to the overall time required for NG neutrons to reach the planetary simulant (for reference, the velocity of the neutrons is 5 cm/ns) and produce gamma photons which, in turn, escaped from planetary simulant and reached the gamma detector. The continuous and uniform signal level under and around the peak is a parasitic background of random coincident detections from gammas generated in the surrounding material (instrument and spacecraft structure/chassis). They are produced by the NG neutrons emitted outside selected solid angle cone but coincided with the time window expected for the gamma signal from the simulant. Therefore, it should be eliminated from the total counting rate leaving only a peak with the background subtracted.

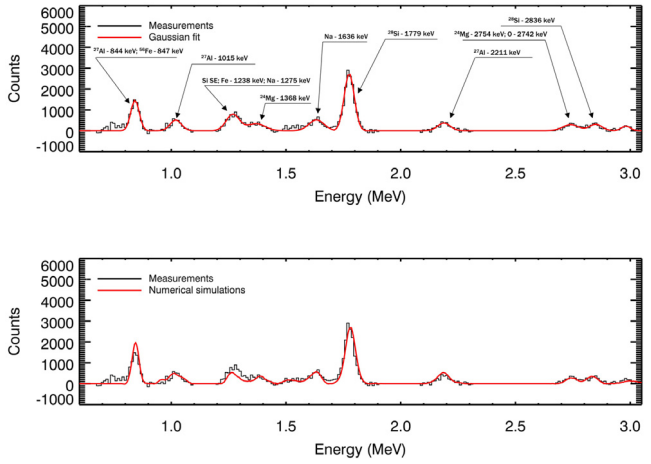

Fig. 5. Gamma peaks (corrected for background) of the major elemental soil constituents deconvolved using the TNM/API approach (black color on all plots). The red line on the top graph shows fitted shapes (Gaussian) of the gamma peaks. The red line on the bottom graph represents numerical simulations. All data are presented for "no lander" configuration. (For interpretation of the references to color in this figure legend, the reader is referred to the web version of this article.)

In the NRA operation mode, the measurements system switched the timing analysis off and recorded all gamma detections regardless of where the gammas came from. As a result, it provided enormous counting statistic but inevitably mixed spacecraft background and subsurface signals. Fig. 4 presents the integrated gamma spectra gathered from the peak area with the background subtracted for the TNM/API mode (top graph) and the integrated gamma spectra acquired in the NRA mode (Fig. 4, bottom graph). The spectra were measured by $LaBr_3$(Ce) spectrometer and presented both for the "no lander" (black color in Fig. 4) and the "lander" (red color in Fig. 4) configurations. Each spectrum has a unique set of gamma lines generated by the primary soil constituents O, Na, Mg, Al, Si, Fe, O, C.

We selected the strongest gamma ray peaks corresponding to the major soil constituting elements, evaluated their peak areas, and defined the statistical uncertainties. The measured accuracy of the peak area characterizes the statistical uncertainty in the evaluation of the elemental concentrations.

To proceed with the data processing of the selected peaks, estimates of the background were carried out. In the integrated spectrum around each selected gamma line, the lower and higher energy intervals were set up to fit the background continuum under the peak area assuming that it varies as a low-order polynomial function. The gamma line profile with the background removed was fitted with a Gaussian shape or with a sum of Gaussians if the gamma lines overlapped each other (see Fig. 5). The retrieved results of the approximation were used to estimate peak area versus background under the peak. The uncertainty of the peak area was defined using the following expression:

$$\Delta = \frac{\sqrt{\delta C^2 + \delta B^2}}{S} \times 100\% \quad (1)$$

where S is the calculated peak area in the range $[E_o - \Delta E, E_o + \Delta E]$, where E_o is defined as the peak position and ΔE is the half width at the half maximum (ΔE is derived from the Gaussian fit). C is the total number of counts including background count rate and B is the sum of background counts only in the range $[E_o - \Delta E, E_o + \Delta E]$. The δC and δB are their uncertainties based on the Poisson statistics.

Previous studies have shown that standard methods of neutron radiation analysis could be efficiently used onboard future landing missions exploring solar system planets and their moons [23,26,27,40]. These methods provide very high counting statistics for the measured gamma spectra accumulated for a limited time of surface operations and could distinguish a set of gamma lines for primary soil constituents.

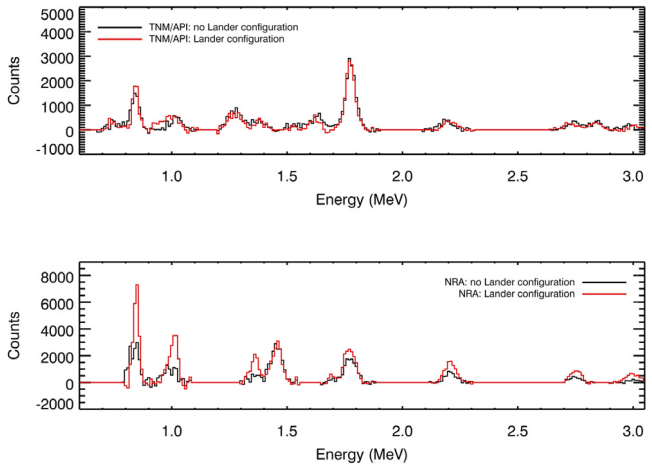

Fig. 6. Background subtracted gamma peaks of major soil constituting elements deconvolved in TNM/API (top graph) and NRA (bottom graph) approaches for "lander" (red color) and "no lander" (black color) configurations . (For interpretation of the references to color in this figure legend, the reader is referred to the web version of this article.)

Nevertheless, the major impact that dramatically influences the interpretation of the observations concerns the signal to noise discrimination and depends on the presence of the surrounding spacecraft materials. Indeed, the visual inspection of the integrated spectra presented in Fig. 4 confirms that the spacecraft material around a gamma detector significantly increases the background for the NRA measurements but does not impact the TNM/API measurements.

The integrated spectrum acquired in the "lander" configuration using standard neutron radiation analysis demonstrates two effects: (1) an additional continuum background is produced under the gamma peaks (see Fig. 4, bottom graph); (2) the intensity of many of the gamma peaks also increases (see Fig. 6, bottom graph). The last phenomenon occurs due to the widespread presence of some "soil" elements in the spacecraft components. The first effect means that the signal-to-noise ratio is worse due to the larger continuum under the gamma lines. The second one means that it is necessary to distinguish between the elemental composition of the soil and the elemental composition of spacecraft. To fix it, a gamma ray spectrometer needs to be evaluated using sophisticated ground calibrations and the experimental data should be verified with numerical simulations. It often occurs that calibration measurements with and without the lander are not technically possible and some compromise should be found to identify the spacecraft elemental composition during available ground tests or during commissioning measurements in space.

In the following we present element by element our analysis and discussion of our findings:

Aluminum. We initiated our analysis using the aluminum gamma lines due to several reasons. First of all, it is known that planetary soils include significant amounts (5%–10%) of this element in the form of Al_2O_3 oxide. Second, aluminum alloys are widely distributed in different spacecraft structures and could significantly increase the intensity of the gamma lines and complicate the evaluation of the true concentration of aluminum in the subsurface. As it was described in Section 2, for our ground tests we specifically added several hundred kilos of aluminum alloys to imitate the material around the gamma spectrometers and produce a parasitic "Al" background in the gamma spectra. The third reason concerns the multiple processes responsible for the generation of the Al gamma lines. Unfortunately, they produce emissions in the energy ranges which coincide with or overlap many characteristic gamma lines from other elements making the evaluation of their concentrations or even identification more difficult.

Excited states of ^{27}Al are produced in inelastic scattering reactions with fast neutrons and then de-excite to the ground state with the emission of 844 keV, 1015 keV, 2211 keV, and 3004 keV. Gamma peaks at these energies are clearly visible in all the spectra plots. Due to limited energy resolution of gamma detectors, the gamma peak at 844 keV is indistinguishable from the gamma peak at 847 keV which is produced by an inelastic scattering reaction with Fe nuclei. It significantly complicates independent detection and evaluation of the iron concentration. In addition to inelastic scattering reactions, continuous neutron irradiation can produce gamma emission through the neutron capture (with thermal neutrons) and neutron activation (decay of short lived isotopes) reactions. Thus, the inelastic scattering of Al peak at 2211 keV overlaps the peak at 2223 keV produced by neutron capture reaction with Hydrogen (the polyethylene layer in the simulant or subsurface water in planetary soils). It means that the separation between H or Al is quite problematic if measurement technique does not separate inelastic scattering and neutron capture reactions. The neutron activation of aluminum occurs through reactions with thermal and fast neutrons. The (n,p) reaction ^{27}Al(n,p) ^{27}Mg with fast neutrons produces short the lived isotope ^{27}Mg (~9.5 min). It beta decays to the excited state of ^{27}Al and then de-excites to the ground state with the emission of the same 844 keV and 1015 keV gamma lines as in the case of inelastic scattering. Another reaction, ^{27}Al(n,α) ^{24}Na with fast neutrons, produces the radioactive isotope ^{24}Na which beta decays to ^{24}Mg with the emission of characteristic gamma lines at 2754 and 1368 keV. They correspond to the de-excitation from the second to the first excited state and then to the ground state and coincide with Mg characteristic gamma lines produced in inelastic scattering reactions. This means that the Mg gamma peaks in the integrated spectra could be polluted by the Al component. The intensity of these lines will vary depending on how much Al is present in the subsurface and in the surrounding spacecraft material. It also depends on the inventory of activated isotopes if time selection analysis to separate inelastic scattering, capture and neutron activation reactions will not be applied. The irradiation with thermal neutrons (the result of the moderation of fast neutrons in polyethylene imitating subsurface water) produces the radioactive isotope aluminum-28 which beta decays to silicon in an excited state with the following de-excitation and emission of 1.78 MeV gamma photons. The last one coincides with gamma emissions observed during inelastic scattering reactions on Si (see considerations below on the detection of Si lines).

Summarizing these examples, one can conclude that the presence of aluminum enriched material around gamma detectors significantly increases both the continuum background and the intensity of many of the gamma lines and provides obvious difficulties in the evaluation of not only Al but also Fe, Mg, and Si abundances in planetary soils.

To conduct a useful space experiment, it is therefore necessary to formulate two strict requirements:

(1) Provide precise discrimination between the background sources and the true signals in the amplitude of the gamma peak;

(2) Conduct science measurements in a way which maximally separates the different processes of gamma emission.

The standard NRA methods, based on continuous neutron irradiation (like it was implemented in our tests), cannot fully meet both these requirements. They cannot distinguish between gamma emissions produced by different types of nuclear reactions and the mixed gamma signals from the object being interrogated and the surrounding environment. It is clearly seen in the spectra measured in the ground tests with the NRA methods for "no lander" and "lander" configurations, see Fig. 4 (bottom plot) and 6 (bottom plot). These Figures show that, in the "lander" configuration in the low energy range, the continuum background increases by ~30% and the intensities of the gamma lines at 844 keV, 1015 keV, 1368 keV, 1779 keV 2211 keV, 2754 keV, and 3004 keV became higher by 1.5–3 times.

On the other hand, requirements were successfully met in TNM/API approach. Ground tests proved that TNM/API measurements are not significantly affected by the background produced in the surrounding materials. It is illustrated in Figs. 4–6. Both the background continuum and the intensity of gamma lines in the "lander" configuration are at

the same levels as were observed in the "no lander" configuration. The ratio between the intensities of all gamma peaks in the "no lander" and the "lander" configurations oscillates around 1 in accordance with statistical uncertainty. It is also important to add that TNM/API helps to eliminate the intrinsic radioactive background of $LaBr_3(Ce^{3+})$, such as ^{138}La gamma emission at 1471 keV. This peak is easily visible in the NRA measurements (see Figs. 4 and 6, bottom graph) and completely disappears in the spectra acquired by the TNM/API method (see Figs. 4 and 6, top graph).

The TNM/API measurements allowed us to achieve a statistical uncertainty of about 4.7% for the Al/Fe peak at 844–847 keV, 10.5% for the Al peak at 1015 keV, 9.0% for the Al peak at 2211 keV, and 13.3% for the Al peak at 3004 keV in accordance with Eq. (1).

The NRA measurements in the "lander" configuration could distinguish the Al/Fe peak at 844–847 keV, the Al peak at 1015 keV, and the Al peak at 2211 keV with statistical uncertainties of 4.6%, 9.7%, and 7.8% respectively. It accounts for corrections to the true intensities of the Al gamma peaks that originated in the planetary simulant. This correction is done using the "no lander" measurements. The gamma peaks at 2211 keV and 3004 keV could not be used for the explicit identification of the Al abundance in the planetary soil simulant. The Al gamma peak at 2211 keV significantly overlaps H capture line at 2223 keV both in the "no lander" and the "lander" configurations. The Al gamma peak at 3004 keV is not detectable in the "no lander configuration" and its amplitude in the "lander" configuration fully accounts for the abundance of Al in the spacecraft materials.

Thus, TNM/API provides "pure" observations of subsurface Al but is affected by low counting statistic and requires longer observation times to increase accuracy. The NRA method provides better statistical uncertainties but strongly depends on the correct deconvolution of the gamma peak between the subsurface and spacecraft components. This method cannot resolve and evaluate all the Al gamma peaks because of their overlap with other gamma emission peaks in this energy range.

Silicon. The concentration of Si in planetary soils may exceed 20%–40%. In the integrated gamma spectra Si is detectable using several characteristic gamma lines. The strongest gamma emission is produced at 1779 keV via inelastic scattering reaction. It could be followed by a single escape peak at 1268 keV. These gamma peaks are both observed and have the same amplitudes in the TNM/API spectra acquired in the "no lander" and the "lander" configurations. The projected TNM/API precision in estimating the Si concentration is about 1.9% (see Table 1). For NRA methods, in addition to inelastic scattering the main gamma peak could also be produced via the neutron activation reaction $^{28}Si(n,p)\ ^{28}Al$ which creates an ^{28}Al isotope with a half-life of 2.24 min. The ^{28}Al beta decays to the excited state ^{28}Si followed by the de-excitation to the ground state with an emission at 1779 keV. It was pointed out above that the presence of Al in spacecraft structure around gamma detectors affects many gamma lines. The neutron capture reaction with ^{27}Al produces a short lived isotope with the same characteristic emission at 1779 keV. As a result, the intensities of the gamma peak at this energy for the "no lander" and the "lander" configurations are significantly different. In the NRA measurements, the amplitude of the gamma peak increases approximately by 30% for the "lander" configuration. If the Al contribution is removed the projected accuracy of the estimation of silicon concentration is about 4% for the "lander" configuration (see Table 1).

Iron. Fe is another chemical element usually found in planetary soils. The model of the planetary soil used in our ground tests contains up to 12.5% of Fe by mass fraction. The inelastic scattering reactions with fast neutrons produce excited states of ^{56}Fe with subsequent de-excitation to the ground state with the emission of gamma rays with energies 847 keV (yield = 99%), 1811 keV (yield = 27%), and 2113 keV (yield = 14%). The same gamma emission is also initiated in the neutron activation reaction $^{56}Fe(n,p)\ ^{56}Mn$ which produces ^{56}Mn isotope decaying with a half-life of about 2.6 h. Considering that the spectral resolution of $LaBr_3(Ce^{3+})$ is not perfect, one may argue that all peaks at these energies significantly overlap Al gamma lines at 844 keV, 2211 keV and the Si gamma line at 1779 keV (see paragraphs above). This means that the independent evaluation of Fe concentration is difficult, and we shall proceed with a model dependent analysis based on known concentrations of other elements. Thus, the Al concentration could be derived from the analysis of 1015 keV, 2211 keV, and 3004 keV gamma peaks. The alternative selection could be done using the timing analysis of passive observations in later time windows after the neutron irradiation is stopped because the half-lives of isotopes produced via reaction with Al and Si are significantly shorter than the decay of the ^{56}Mn isotope (minutes vs hours), see [23,40]. The preference for TNM/API is that it could sustain a constant ratio between Al and Fe contributions in the intensity of the measured gamma peaks. This ratio depends on the soil composition and does not depend on how much Al or Fe there is in the surrounding spacecraft material. Tests have shown that the amplitude of the gamma peak in the 844–847 keV energy range is the same for the "lander" and the "no lander" configurations in the case of TNM/API measurements and significantly different for NRA measurements.

Sodium. Na is a substantial mass fraction (about 8%) in our model of planetary material. In the integrated spectra, the irradiation of the planetary material with fast neutrons could produce gamma peaks at 440 keV, 1636 keV, and 1275 keV via interactions with the ^{23}Na isotope. Due to the overloading of the data processing electronics, the energy range below 600 keV was excluded from the analysis. The gamma peaks at 1636 keV and 1275 keV were detected in TNM/API measurements with a high confidence but the second one overlaps the Fe gamma line (1238 keV) and the single escape peak from Si (1268 keV). In the NRA measurements, the peaks at 1636 keV and 1275 keV are not very visible due to the high level of the continuum background. Since Na is not abundant in the surrounding spacecraft materials, the transition from "no lander" to "lander" configuration does not change the intensity of sodium gamma peaks. The highest expected precision in all our measurements is about 8% (gamma peak at 1636 keV).

Oxygen. The last element examined in the current work was O. It is the most abundant element because planetary soils include mixtures of various oxides. It is not, however, as important a geochemical marker as many other soil constituents but its analysis is required to understand how these elements are bonded in the oxides. O is easily detected by multiple characteristic gamma lines scattered across a wide energy range. For inelastic scattering reactions it includes a forest of strong gamma lines at 2742 keV, 3684 keV, 3854 keV, 6130 keV, and 7113 keV followed by several single and double escape peaks. These lines are resolved with a very high confidence both by the NRA and the TNM/API.

5. Numerical simulations

We used the Monte Carlo N-Particle eXtended code (MCNPX is a numerical code widely used for space gamma/neutron modeling applications, see [41]) to support some of our test measurements with numerical simulations and to compare the measured intensity of characteristic gamma lines with the expectations derived from our modeling approach. In our model we simulated the neutron irradiation conditions and created a numerical model of the planetary material simulant with an exact description of its structure and elemental composition. The measurement system was modeled in part for the $LaBr_3(Ce^{3+})$ scintillation crystal and includes its configuration, volume, and sensitivity. The calculations were carried out as a two-step procedure. A simulation of the gamma emission in the simulant material due to neutron irradiation was completed during the first step. Its subsequent transport to the detector and the interactions in the detector volume constituted the final step. The procedure implemented reproduces the gamma counts in accordance with the detector's efficiency using the pulse-height tally in MCNP. To compare the ideal model spectrum with observations, it was smoothed with an energy-variable filter to simulate

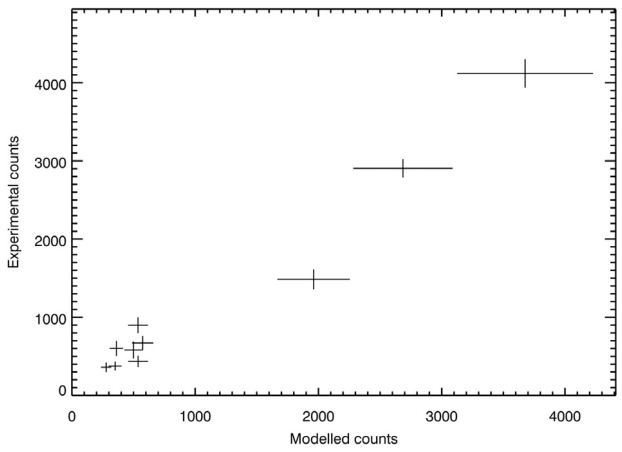

Fig. 7. Correlation between experimental and modeled intensities of gamma peaks corresponding to major constituent elements of the soil. The comparison is done for the TNM/API measurements in the "no lander" configurations (see also Fig. 5, bottom graph).

the true energy resolution of the $LaBr_3(Ce^{3+})$ detector as determined from the calibrations. The primary goal was to consider a simple case and understand how modeling predictions of the gamma measurements in "no lander" configuration is close to the observations based on the TNM/API methods. We simulated the timing scheme for TNM/API measurements by tracking the fast neutrons and their interactions with simulant material nuclei. The whole process was limited by a very short observation period as in the real experiment to account for gamma photon production in the planetary soil simulant via inelastic scattering reactions and their further transport to the gamma detector.

The comparison between the observed and modeled gamma peaks with the background subtracted is presented in Fig. 5. It was performed for the TNM/API test in the "no lander" configuration and showed an appropriate agreement with observations, except perhaps gamma peaks at 844–847 keV and 1240–1260 keV energy ranges. The first one presents mixture of Al and Fe lines and the second one is a heavily overlapping of several weak gamma lines from Na, Fe and single escape of Si (at 1779 kev). The deviation of model predictions from the observations at strong gamma peak around 844–847 keV could be explained by the lower efficiency of detector and detector electronics due to dead time, non-detailed modeling of detector enclosure (which may attenuate gammas at lower energies) and some uncertainties in numerical simulations (simulation of gamma production processes and variations in cross sections libraries). The correlation between measured and modeled intensities of gamma lines is shown in Fig. 7. A Pearson Correlation Coefficient was calculated for this comparison. It is close to 1, which indicates a high level of correlation.

6. Discussion and conclusions

The rapid development of background-suppressed TNM/API technologies for 3-D analysis and their consequent broad implementation for a variety of tasks encourage us to test their applicability for space experiments. These technologies may open new possibilities and perspectives for the future surface landers on the different planets of the Solar system—especially for the comprehensive analysis of planetary subsurfaces. Two major and very promising improvements are anticipated if this approach can be proved and adapted to the requirements for a space experiment.

The first one concerns the reliable identification of the bulk subsurface elemental composition and of the background generated by the surrounding spacecraft materials. For standard gamma spectroscopy methods it is not as simple a task as one might expect. It requires considerable prelaunch efforts (to perform complicated calibrations) and even more efforts when the first data come to the ground followed by a very sophisticated data analysis.

The second improvement provided by the TNM/API is the 3-D description of the subsurface under the lander. In many cases it is extremely important because the subsurface represents a mixture of layered deposits which need to be evaluated in detail to characterize planetary evolution. Using only standard methods of observations this goal is very difficult to achieve. Indeed, it requires a combination of measurements and model dependent data deconvolution while the TNM/API can do it via direct measurements.

In ground tests in the initial stage, we have focused on the first task and have considered potential advantages and disadvantages of the TNM/API versus standard NRA methods to correctly evaluate the subsurface bulk elemental composition. To reach this goal we conducted tests in the so called "no lander" and "lander" configurations. The "no lander" configuration is close to the ideal case where the gamma detector is alone or located far away from the main spacecraft body. For the "lander" configuration we have added significant amounts of Al alloy material around the gamma spectrometer to imitate the actual spacecraft environment/configuration.

The ground tests proved that significant suppression of the parasitic background onboard the spacecraft was possible. The TNM/API spectra acquired in the "no lander" and the "lander" configurations are practically identical. This means that two important negative factors impacting standard gamma spectroscopy observations are under control during the TNM/API measurements: the level of background continuum and the intensity of the detected gamma lines. The surrounding materials produce and scatter gamma photons and significantly increase the continuum gamma emission. This factor leads to larger uncertainties in the estimation of the gamma peak intensities due to a lower signal-to-noise ratio. As a result, the accuracy in the evaluation of elemental abundances is also goes down. Another impact is that the same chemical elements can be found both in subsurface and in the spacecraft structure. This is an even worse problem because in this case the amplitudes of the many gamma peaks studied will be modified/polluted by significant contributions from the spacecraft elemental abundances. If this factor is not accurately taken into account, misleading information about the subsurface composition will be provided. The ground tests showed that for the standard NRA methods this was the major issue. For example, the Al gamma lines in the integrated NRA spectrum increased their intensity up to 3 times after adding several hundred kilos of Al-rich material imitating the spacecraft structure. Moreover, due to various emission processes (inelastic scattering, neutron capture, and neutron activation reactions), Al gamma lines coincided with or overlapped gamma emissions from other soil constituents such as Fe, Si, ans Mg, making their evaluation significantly difficult. A possible way to fix this problem is to evaluate the spacecraft response during ground calibrations and to follow up with numerical modeling. A more radical proposal is based on a special instrument design where the gamma detector is mounted on a boom that places the sensor far from the main spacecraft body. Unfortunately, these solutions require considerable efforts and resources that are not always possible.

Our results imply that the TNM/API can avoid these issues. If the measurement system is integrated at the bottom of the lander, it is possible to select a solid angle cone where neutrons will propagate to the subsurface (and gammas from the subsurface to detector) with minimal interactions with spacecraft elements. Another advantage of the TNM/API is that it uses only inelastic scattering reactions. It substantially simplifies the analysis and interpretation of the observed gamma lines. Here it is important to note that some selection between different types of nuclear reactions can be done if the neutron irradiation occurs in a pulsing mode and the spectra are acquired during the neutron pulse (mostly inelastic scattering reactions) and between pulses (capture and neutron activation reactions), see [15,23,26,27,40]. It is possible to implement such an analysis in both the NRA and the API/TNT methods.

Nevertheless, the performance of the TNM/API is not absolutely perfect and is substantially limited by low counting statistics. This

resulted in an extended measurement duration which was required to get an appropriate accuracy. For example, ground tests showed that uncertainty in the estimation of Al peaks at 844 keV and 2211 keV were about 4.7% and 9.0% respectively (see Table 1) but required ~1 h of measurements. The instrument performance could be improved with some optimization of the alpha particle detector (dimension and location), but not dramatically. However, the NRA methods, based on higher counting statistics, can do better (see Table 1) for much shorter observational time. Of course, this only works if spacecraft response is accurately known. Otherwise systematic errors eliminate any advantages of high counting statistic. The lack of counting statistic for the TNM/API can be substantially improved if a gamma spectrometer is integrated as part of the stationary landing platform. In this case, its overall observation time is defined by the duration of the surface mission. The accuracy can be improved by an order of magnitude in this case. For rover missions, the situation is less favorable because measurements of ~1 h duration (as selected for the ground tests) are close to the maximum time limit available at rover stops. This duration can be increased by several times only during special observational campaigns.

In conclusion we would like to note that the "results of voting" between standard gamma spectroscopy methods and the TNM/API are not so unambiguous and evident. They depend on the specific space mission requirements, the available resources, the duration and mobility of the landing module, and ultimately on the technology readiness level of the TNM/API methods needed to develop the space-qualified instrumentation. Nevertheless, we assert that the TNM/API has significant advantages and is a promising alternative to the standard gamma ray spectroscopy observations including the current NRA system for future landing missions. The on-going ground tests with prototype instrumentation should be continued to raise its TRL and to investigate and formulate these advantages (including a 3-D analysis of the subsurface) more clearly.

References

[1] W.V. Boynton, W.C. Feldman, I.G. Mitrofanov, L.G. Evans, R.C. Reedy, S.W. Squyres, R. Starr, J. Trombka, C. D'Uston, J.R. Arnold, P.A. Englert, A.E. Metzger, H. Wanke, J. Bruckner, D.M. Drake, C. Shinohara, C. Fellows, D.K. Hamara, K. Harshman, K. Kerry, C. Turner, M. Ward, H. Barthe, K.R. Fuller, S.A. Storms, G.W. Thornton, J.L. Longmire, M.L. Litvak, A.K. Ton'chev, The Mars Odyssey Gamma-Ray Spectrometer instrument suite, Space Sci. Rev. 110 (2004) 37–83.

[2] W.V. Boynton, et al., Concentration of H, Si, Cl, K, Fe, and Th in the low- and mid-latitude regions of Mars, JGR 112 (2006) E12S99, http://dx.doi.org/10.1029/2007JE002887.

[3] W.V. Boynton, W.C. Feldman, S.W. Squyres, T.H. Prettyman, J. Bruckner, L.G. Evans, R.C. Reedy, R. Starr, J.R. Arnold, D.M. Drake, P.A. Englert, A.E. Metzger, I. Mitrofanov, J. Trombka, C. d'Uston, H. Wanke, O. Gasnault, D.K. Hamara, D.M. Janes, R.L. Marcialis, S. Maurice, L. Mikheeva, G.J. Taylor, R. Tokar, C. Shinohara, Distribution of hydrogen in the near surface of Mars: evidence for subsurface ice deposits, Science 297 (2002) 81–85.

[4] Malakhov, et al., Fine Resolution Neutron Detector for ExoMars Trace Gas Orbiter. Instrument and science goals, 40th COSPAR Scientific Assembly, Held 2-10 2014, in Moscow, Russia, Abstract B0.2-19-14, 2014.

[5] L.G. Evans, et al., Major-element abundances on the surface of Mercury: Results from the MESSENGER Gamma-Ray Spectrometer, J. Geophys. Res. 117 (2012) CiteID E00L07.

[6] T.H. Prettyman, et al., Elemental mapping by dawn reveals exogenic H in Vesta's regolith, Science 338 (2012) 242.

[7] N. Hasebe, et al., High performance germanium gamma-ray spectrometer on lunar polar orbiter SELENE (KAGUYA), Trans. Space Technol. Japan 7 (2010) Pk_35-Pk_41.

[8] J.O. Goldsten, E.A. Rhodes, W.V. Boynton, W.C. Feldman, D.J. Lawrence, J. Trombka, D.M. Smith, L.G. Evans, J. White, N.W. Madden, P.C. Berg, G.A. Murphy, R.S. Gurnee, K. Strohbehn, B.D. Williams, E.D. Schaefer, C.A. Monaco, C.P. Cork, J.D. Eckels, W.O. Miller, M.T. Burks, L.B. Hagler, S.J. DeTeresa, M.C. Witte, The MESSENGER Gamma-Ray and Neutron Spectrometer, Space Sci. Rev. 131 (2007) 339–391.

[9] Mitrofanov, et al., The Mercury Gamma and Neutron Spectrometer (MGNS) on board the Planetary Orbiter of the BepiColombo mission, Planet. Space Sci. 58 (2010) 116–124.

[10] P.N. Peplowski, Compositional variability on the surface of 4 Vesta revealed through GRaND measurements of high-energy gamma rays, Meteorit. Planet. Sci. 48 (11) (2013) 2252–2270.

[11] T.H. Prettyman, et al., Elemental composition of the lunar surface: Analysis of gamma ray spectroscopy data from Lunar Prospector, J. Geophys. Res. 111 (E12) (2006) CiteID E12007.

[12] T.H. Prettyman, et al., Dawn's gamma ray and neutron detector, Space Sci. Rev. 163 (1–4) (2011) 371–459.

[13] J.P. Grotzinger, et al., Mars science laboratory mission and science investigation, Space Sci. Rev. 170 (2012) 5–56, http://dx.doi.org/10.1007/s11214-012-9892-2.

[14] J.L. Vago, et al., Habitability on early mars and the search for biosignatures with the exomars rover, Astrobiology 17 (2017) http://dx.doi.org/10.1089/ast.2016.1533.

[15] J.G. Bodnarik, et al., Time-resolved neutron/gamma-ray data acquisition for in situ subsurface geochemistry, Nucl. Instrum. Methods Phys. Res. A 707 (2013) 135–142.

[16] D.V. Golovin, et al., Neutron activation analysis on the surface of the Moon and other terrestrial planets, 40th COSPAR Scientific Assembly. Held 2-10 2014, in Moscow, Russia, Abstract B0.1-43-14.

[17] I. Jun, W. Kim, M. Smith, I.G. Mitrofanov, M.L. Litvak, A study of Venus surface elemental composition from 14 MeV neutron induced gamma ray spectroscopy: Activation analysis, Nucl. Instrum. Methods Phys. Res. A 629 (2010) 140.

[18] M.L. Litvak, et al., Ground tests with active neutron instrumentation for the planetary science missions, Nucl. Instrum. Methods Phys. Res. A788 (2015) 194–202.

[19] I.G.I. Mitrofanov, Neutron -Activated Gamma Ray Spectrometer (NAGRS) for the Venus Surface and Atmosphere Geochemical Explorer (SAGE) mission, European Planetary Science Congress 2010, held 20-24 September in Rome, Italy, 264, 2011.

[20] I.G. Mitrofanov, M.L. Litvak, Yu. I. Barmakov, A. Behar, Yu. I. Bobrovnitsky, E.P. Bogolubov, W.V. Boynton, K. Harshman, E. Kan, A.S. Kozyrev, R.O. Kuzmin, A.V. Malakhov, M.I. Mokrousov, V.I. Ryzhkov, A.B. Sanin, G.A. Smirnov, V.N. Shvetsov, G.N. Timoshenko, T.M. Tomilina, V.I. Tret'yakov, A.B. Varenikov, V. Vostrukhin, Experiment for measurements of Dynamic Albedo of Neutrons (DAN) onboard NASA's Mars Science Laboratory, Space Sci. Rev. 170 (1–4) (2012) 559–582.

[21] Nikiforov, et al., Subsurface water observations on Mars: From DAN/Curiosity to Adron-RM/ExoMars, 40th COSPAR Scientific Assembly. Held 2-10 2014, in Moscow, Russia, Abstract B0.2-37-14, 2014.

[22] J. Bruckner, et al., Neutron-induced gamma ray spectroscopy: Simulations for chemical mapping of planetary surfaces, J. Geophys. Res. 92 (B4) (1987) E603–E616.

[23] M.L. Litvak, et al., Implementation of gamma-ray instrumentation for solid solar system bodies using neutron activation method, Nucl. Instrum. Methods Phys. Res. A822 (2016) 112–124.

[24] J.W. Mandler, Continued Development of the Combined pulsed neutron experiment (CPNE) for Lunar and Planetary Surfaces, Final Report, 15 1971–23, 1972.

[25] W.R. Mills Jr., W.W. Givens, Neutron Die-Away Experiment for Lunar and Planetary Surface Analysis, Final Report, 26 1966–26, 1967.

[26] A. Parsons, et al., Nucl. Instrum. Methods A 652 (2011) 674.

[27] A. Parsons, et al., Subsurface in situ elemental surface composition measurements with PING, 2013 IEEE Aerospace Conference, Big Sky, MT, 2-9 March, 2013 (2013) pp. 1-11.

[28] V. Valkovic, et al., Nucl. Instrum. Methods A703 (2013) 133.

[29] M.L. Litvak, et al., Hydrogen and chlorine abundances in the Kimberley formation of Gale crater measured by the DAN instrument on board the Mars Science Laboratory Curiosity rover, JGR (2016) http://dx.doi.org/10.1002/2015JE004960.

[30] M.L. Litvak, I.G. Mitrofanov, A.B. Sanin, D.I. Lisov, A. Behar, W.V. Boynton, L. Deflores, F. Fedosov, D. Golovin, C. Hardgrove, K. Harshman, I. Jun, A.S. Kozyrev, R.O. Kuzmin, A. Malakhov, R. Milliken, M.A. Mischna, J.E. Moersch, M. Mokrousov, S. Nikiforov, V.N. Shvetsov, K. Stack, R. Starr, C. Tate, V.I. Tret'yakov, A. Vostrukhin, Local variations of bulk hydrogen and chlorine content measured at the contact between the sheepbed and gillespie lake units in yellowknife bay, gale crater, using the DAN instrument onboard curiosity, JGR 119 (6) (2014) 1259–1275.

[31] M.L. Litvak, I.G. Mitrofanov, Yu. N. Barmakov, A. Behar, A. Bitulev, Yu. Bobrovnitsky, E.P. Bogolubov, W.V. Boynton, S.I. Bragin, S. Churin, A.S. Grebennikov, A. Konovalov, A.S. Kozyrev, I.G. Kurdumov, A. Krylov, Yu. P. Kuznetsov, A.V. Malakhov, M.I. Mokrousov, V.I. Ryzhkov, A.B. Sanin, V.N. Shvetsov, G.A. Smirnov, S. Sholeninov, G.N. Timoshenko, T.M. Tomilina, D.V. Tuvakin, V.I. Tretyakov, V.S. Troshin, V.N. Uvarov, A. Varenikov, A. Vostrukhin, The dynamic albedo of neutrons (DAN) experiment NASA's 2009 mars science laboratory, Astrobiology 8 (3) (2008) 605–612.

[32] I.G. Mitrofanov, M.L. Litvak, A.B. Sanin, R.D. Starr, D.I. Lisov, R.O. Kuzmin, A. Behar, W.V. Boynton, C. Hardgrove, K. Harshman, I. Jun, R.E. Milliken, M.A. Mischna, J.E. Moersch, C.G. Tate, Water and chlorine content in the Martian soil along the first 1900 m of the Curiosity rover traverse as estimated by the DAN instrument, JGR 119 (7) (2014) 1579–1596.

[33] V.N. Shvetsov, et al., Ground tests of the Dynamic Albedo of Neutron instrument operation in the passive mode with a Martian soil model, Nucl. Instrum. Methods Phys. Res. A 861 (2017) 1–6.

[34] A. Beyerle, J.P. Hurley, Nucl. Instrum. Methods A299 (1990) 458.

[35] V.M. Bystritsky, et al., DViN–stationary setup for identification of explosives, Phys. Part. Nucl. Lett. 5 (2008) 441–446.

[36] V.M. Bystritsky, et al., Stationary setup for identifying explosives using the tagged neutron method, Phys. Part. Nucl. Lett. 10 (2013) 442–446.
[37] N.E. Ipe, et al., A cargo inspection system based on pulsed fast neutron analysis (PFNATM), Radiat. Prot. Dosim. 116 (2005) 343–346.
[38] Alexakhin V. Yu, et al., Use of the tagged neutron technique for detecting dangerous underwater substances, Phys. Part. Nucl. Lett. 10 (2013) 860–867.
[39] Alexakhin V. Yu, et al., Detection of diamonds in kimberlite by the tagged neutron method, Nucl. Instrum. Methods Phys. Res. A 785 (2015) 9–13.
[40] M.L. Litvak, et al., Ground tests with prototype of CeBr3 active gamma ray spectrometer proposed for future venus surface missions, Nucl. Instrum. Methods Phys. Res. A 848 (2017) 9–18.
[41] D.B. Pelowitz, MCNPX User's Manual, Version 2.7.0, LANL Report LA-CP-11-00438, Los Alamos National Laboratory, 2011.